



HAL
open science

Dynamic Functional Connectivity in Adolescence-Onset Major Depression: Relationships With Severity and Symptom Dimensions.

Rocco Marchitelli, Marie-Laure Paillère-Martinot, Nadège Bourvis, Christophe Guerin-Langlois, Amélie Kipman, Christian Trichard, Marie Douniol, Coline Stordeur, André Galinowski, Irina Filippi, et al.

► To cite this version:

Rocco Marchitelli, Marie-Laure Paillère-Martinot, Nadège Bourvis, Christophe Guerin-Langlois, Amélie Kipman, et al.. Dynamic Functional Connectivity in Adolescence-Onset Major Depression: Relationships With Severity and Symptom Dimensions.. *Biological Psychiatry: Cognitive Neuroscience and Neuroimaging*, 2021, 10.1016/j.bpsc.2021.05.003 . hal-03471648

HAL Id: hal-03471648

<https://hal.science/hal-03471648>

Submitted on 22 Jul 2024

HAL is a multi-disciplinary open access archive for the deposit and dissemination of scientific research documents, whether they are published or not. The documents may come from teaching and research institutions in France or abroad, or from public or private research centers.

L'archive ouverte pluridisciplinaire **HAL**, est destinée au dépôt et à la diffusion de documents scientifiques de niveau recherche, publiés ou non, émanant des établissements d'enseignement et de recherche français ou étrangers, des laboratoires publics ou privés.



Distributed under a Creative Commons Attribution - NonCommercial 4.0 International License

Dynamic functional connectivity in adolescence-onset major depression: relationships with severity and symptom dimensions

Rocco Marchitelli, PhD¹, Marie-Laure Paillère-Martinot, MD, PhD^{1,2}, Nadège Bourvis, MD, PhD³, Christophe Guerin-Langlois, Psych⁴, Amélie Kipman, MD⁵, Christian Trichard, MD, PhD^{1,6}, Marie Douniol, MD⁷, Coline Stordeur, MD⁸, André Galinowski, MD¹, Irina Filippi, PhD¹, Gilles Bertschy, MD, PhD⁹, Sébastien Weibel, MD, PhD⁹, Bernard Granger, MD, PhD^{1,10}, Frédéric Limosin, MD, PhD⁴, David Cohen, MD, PhD², Jean-Luc Martinot*, MD, PhD¹, Eric Artiges*, MD, PhD^{1,6}.

¹INSERM U1299 "Trajectoires développementales & psychiatrie", University Paris-Saclay, Ecole Normale Supérieure Paris-Saclay, CNRS; Centre Borelli, Gif-sur-Yvette, France; ²AP-HP, Sorbonne Université, Department of Child and Adolescent Psychiatry, Pitié-Salpêtrière Hospital, Paris, France; ³Maison des Adolescents du Var (MDA83), Pôle de Psychiatrie Infanto-Juvenile, Centre Hospitalier Intercommunal Toulon la Seyne (CHITS), Toulon, France; ⁴APHP, Department of Psychiatry and Addictology, Hôpital Corentin Celton, Paris Descartes University, Paris, France. ⁵APHP, Psychiatry department, Hôtel-Dieu hospital, Paris, France; ⁶EPS Barthélémy Durand, Psychiatry Department, Etampes, France; ⁷Centre médico-psychologique pour adolescents, Sceaux, France; ⁸Hôpital Robert Debré, Service de Psychiatrie de l'Enfant et de l'Adolescent, Paris, France; ⁹Strasbourg University, Psychiatry department, hôpital Civil de Strasbourg, and INSERM U 1114, Strasbourg, France; ¹⁰AP-HP, Psychiatry Department, Tarnier Hospital, University Paris Descartes, Paris, France.

*Contributed equally

Corresponding Author #1

Jean-Luc Martinot, MD, PhD

INSERM U1299 "Trajectoires développementales & psychiatrie"

Digiteo - Labs, Bâtiment 660 Claude Shannon,

Avenue des Sciences 91190 Gif-sur-Yvette, France.

Telephone and fax +33169154410

e-mail: jean-luc.martinot@inserm.fr

Corresponding Author #2

Rocco Marchitelli, PhD

INSERM U1299 "Trajectoires développementales & psychiatrie"

Digiteo - Labs, Bâtiment 660 Claude Shannon,

Avenue des Sciences 91190 Gif-sur-Yvette, France.

Telephone and fax +393773072859

e-mail: rocco.marchitelli@inserm.fr

Keywords: resting-state fMRI, dynamic functional connectivity, major depressive disorder, independent component analysis, Montgomery-Asberg depression rating scale, functional chronnectome

Abstract

Background: The spatial functional chronnectome is an innovative mathematical model designed to capture dynamic features in the organization of brain function derived from resting-state functional magnetic resonance imaging (rs-fMRI) data. Measurements of dynamic functional connectivity (dFC) have been developed from this model to quantify the brain dynamical self-reconfigurations at different spatial and temporal scales. This study examined whether two spatiotemporal dFC quantifications were linked to late adolescence-onset major depressive disorder (AO-MDD), and scaled with depression and symptom severity measured with the Montgomery-Asberg depression rating scale (MADRS). **Methods:** Thirty-five AO-MDD patients (21 ± 6 y) and fifty-three age- and gender-matched healthy young participants (20 ± 3 y) underwent 3T MRI structural and rs-fMRI acquisitions. The chronnectome here comprised seven individualized functional networks portrayed along 132 temporal overlapping windows, each framing 110s of resting brain activity. **Results:** Based on voxelwise analyses, AO-MDD patients demonstrated significantly reduced temporal variability within the bilateral prefrontal cortex in five functional networks including the limbic network, the default-mode network (DMN) and frontoparietal network (FPN). Furthermore, the limbic network appeared to be particularly involved in this sample, and was associated with MADRS scores, and its progressive dynamic inflexibility was linked to sadness. DMN and FPN dynamics scaled with negative thoughts and neurovegetative symptoms, respectively. **Conclusions:** This triple-network imbalance could delay spatiotemporal integration, while across-subject symptom variability would be network-specific. Therefore, the present approach supports that brain network dynamics underlie patients' symptom heterogeneity in AO-MDD.

1. Introduction

Major depressive disorder (MDD) is a prevalent chronic episodically-recurrent disorder (1) that presents core symptoms of profound sadness and anhedonia, irritability, indecisiveness and recurrent suicidal ideation (2) associated with sleep and eating disturbances, physical fatigue and comorbid anxiety symptoms (3). First MDD episodes often occur prior to adulthood with adolescence-onset MDD (AO-MDD) patients being more likely to suffer from exacerbated recurrent episodes and poorer social and occupational function throughout lifespan (4, 5). Task-free neuroimaging studies conducted using resting-state functional magnetic resonance imaging (rs-fMRI) suggest that MDD arises from abnormal synchronism in spontaneous brain activity in neural circuitries implicated in emotional processing and regulation (6-11). Although their neural-behavioral mechanisms remain uncertain, they could reflect adolescence developmental changes that might contribute to the persistence of depression risk through young adulthood (12).

Abnormal synchrony, commonly quantified using functional connectivity (FC) methods (13), is connoted by disrupted FC in the anterior Default-mode network (DMN) and Frontoparietal network (FPN) whereas the subgenual cingulate augments FC within the Limbic network which can furthermore return to normal after pharmacological treatment (14, 15). Many studies have therefore implemented such network-based approaches to investigate the value of FC as an endogenous imaging biomarker of MDD (16, 17), in terms of disease severity (18, 19), qualitative symptoms (20), and pharmaceutical (21) or psychotherapeutic interventions (22, 23).

Taken together, these findings promote the development of imaging biomarkers to support psychiatric diagnosis and interpret MDD symptomatology (24). However, commonly adopted FC methods assume static brain networks' configurations, averaged over the scanning time. This assumption might impact FC sensitivity to MDD pathology, leading to inconsistent or incomparable findings, thence discouraging the clinical usage of FC from rs-fMRI (25, 26). The functional chronnectome approach suggests that brain FC is dynamic in nature in that its intrinsic neural

organization embraces stationary as well as non-stationary events (26). This approach has revealed that several resting-state brain networks transit across different discrete, recurrent, spatiotemporal configurations, consistent across healthy subjects (26). This dynamic FC (dFC) approach assumes that during rest these spatiotemporal configurations would reflect dynamic interactions across brain networks for supporting internally oriented cognition (27, 28). Therefore, dFC might be useful to assess intrinsic functional brain organization (29), neural-behavioral relationships (31-33) and their alterations in MDD (34-36).

In this dynamic rs-fMRI study, we contributed to this stream of research probing the temporal evolution of the functional connectome in young AO-MDD patients, evaluating its linear relationships with depression severity as assessed by the clinician-rated Montgomery-Asberg Depression Rating Scale (MADRS), a robust psychometric instrument used to track disease staging and recovery (37) (Montgomery-Asberg Depression Rating Scale, RRID:SCR_003690). Moreover, we examined dynamic neural-behavioral covariation at the symptom-level selecting a multifactorial hierarchical MADRS model (38) to further investigate relationships between dFC and MDD symptom dimensions. To maximize MADRS sensitivity, we defined a clinically variegated sample of young patients also including underage individuals at different stages of disease and treatment course. To attenuate potential dFC biases due to sample variability, we used a spatial chronnectome model (29) that exploits group independent component analysis (gICA) to generate time-resolved individual coupling maps for any resting-state functional network.

2. Methods & Materials

2.1. Subjects & psychometrics

Thirty-five AO-MDD patients and 53 healthy participants were herein studied (**Table 1**). Data were retrieved from two conjoined studies of AO-MDD in young adults and adolescents, respectively. The former one provided 15 patients and 2 control subjects, while the latter provided datasets for 20 patients and 22 healthy participants. The remaining ones, 29 healthy participants, were retrieved from the IMAGEN database (<http://imagen-europe.com>), matched with patients for age and gender. All participants were included and scanned in the same center at the same time period.

All patients referred to had experienced first depressive symptoms during adolescence when they received a diagnosis of major depressive disorder according to the DSM-IV-TR from psychiatrists either in hospitalization wards or outpatient clinics (**Table 1**). These young patients were investigated at various stages of their depressive episodes to maximize sample variability. Thus, at scanning time, 19 patients were in their first episode of illness according to Mini-International Neuropsychiatric Interview (30) (M.I.N.I.). The 16 other ones were in their second or third episode. Sixteen patients, of whom 8 in their first episode of illness, were treated with selective serotonin reuptake inhibitors (SSRIs) and 4 patients (1 first-episode) received serotonin–norepinephrine reuptake inhibitors (SNRIs). One first-episode patient had received noradrenergic and specific serotonergic antidepressant (NaSSa). Eight SSRI and 2 SNRI-treated cases also received benzodiazepines (Alprazolam, Bromazepam, Prazepam) to reduce excessive anxiety. Medicated patients were stabilized and showed no discontinuation symptoms.

Depression severity was assessed by MADRS (Montgomery-Asberg Depression Rating Scale, RRID:SCR_003690) administration before the scanning session by an experienced research psychiatrist (JLM, EA). The MADRS is a clinician-rated seven-point scale, based on 10 items: apparent sadness; reported sadness; inner tension; reduced sleep; reduced appetite; concentration

difficulties; lassitude; inability to feel; pessimistic and suicidal thoughts. The total MADRS score across these items ranges from 0 to 60, with higher scores reflecting greater depression severity. A multifactorial time- and gender-invariant model of MADRS was used to differentiate MDD symptoms into four sub-dimensions, namely sadness (apparent and reported sadness), neurovegetative symptoms (inner tension, reduced sleep and appetite), detachment symptoms (concentration difficulties, lassitude and inability to feel) and negative thoughts (pessimistic and suicidal thoughts) (38). Each MADRS sub-dimension was assessed via the straight sum across its items.

Healthy participants had not experienced any past or current MDD episode, according to M.I.N.I. criteria. MADRS scores were rated by a trained psychiatrist (JLM, EA) in 25 healthy controls. The self-rated versions of the Centre for Epidemiological Studies Depression (39) (CES-D) or the Adolescent Depression Rating Scale (ADRS) (40) were administered as alternative in the remaining participants depending on their age.

Exclusion criteria included pregnancy, alcohol or substance abuse or dependence in the past six months, electroconvulsive therapy treatment in the past six months, any present medical somatic condition, history of epileptic seizures, history of bipolarity or other psychiatric, neurological disorders or substantial brain damage, and contraindication to magnetic fields, according to established safety criteria. Written informed consent had been obtained from all participants or their parents in case of individuals aged less than 18. The study had obtained approval from the Bicêtre ethics committee Ile de France 7.

2.2. Data acquisition and preprocessing

Participants underwent a single ~45 min neuroimaging session using a 3T MR Siemens Prisma (Siemens Healthcare, Erlangen, Germany) at Center for NeuroImaging Research (CENIR) within the Institut du Cerveau (ICM), Paris. All participants had been scanned on the same machine, using the same head-coil and MR sequences conformed to the IMAGEN acquisition protocol. In

particular, all participants had undergone an initial magnetization-prepared radio-frequency rapid gradient-echo (MPRAGE) volume acquisition (TR=2300ms, TE=2.93ms, FA=9°, TI=900ms, voxel-size=1.1mm³, duration=10min). The MR acquisition included eyes-closed resting-state blood-oxygen level-dependent echo-planar imaging (BOLD-EPI) to image brain function (TR=2200ms, TE=30ms, FA=75°, voxel-size=2.4mm³, length=187, duration=7min). Participants were asked to remain as still as they could during the scanning time, and relax. They were soothed and recommended not to fall asleep during rs-fMRI acquisitions.

Neuroimaging processing was performed in AFNI (41) (Analysis of Functional NeuroImages, RRID:SCR_005927) and FSL (42) (FSL, RRID:SCR_002823). Image preprocessing steps were described in previous works (43). For clarity, T1-weighted MPRAGE and BOLD-EPI functional images were aligned and preprocessed in their original space. Rigid-body head-motion correction was performed as implemented in FSL. Multiple regressions of six displacement time-courses, their derivatives and mean regional white matter (WM) and cerebral spinal fluid (CSF) were conducted for effective motion and physiological denoising of BOLD-EPI data (43). After confound regression, AFNI's 3dDespike was additionally performed to account for micro-movements. Subjects exceeding either 1.5mm in translations, 1.25 degrees in rotation were discarded from the study (44). To summarize head-motion in each participant, framewise displacements (FD) were measured. After being preprocessed, individual BOLD-EPI data were linearly normalized to 2-mm isotropic Montreal Neurological Institute (MNI) template using 12 degrees-of-freedom affine transformation.

2.3. Characterizing group-level functional networks

Functional imaging data were decomposed into group functional networks using group-ICA algorithms as implemented in MELODIC. Temporal concatenation of preprocessed BOLD-EPI functional data across subjects (N=88) preceded ICA decomposition into 20 spatial and temporal components. To exclude components related to physiologic, motion and scanner noise artifacts,

each stochastic component was spatially compared with 7 external templates (45) namely the DMN, the FPN, the Limbic and Salience networks, the Dorsal-attention network (DAN), the Visual and Sensory-motor networks. The 7 best-matched components, so defined by their highest and lowest degree of positive z-scores respectively within and outside each template, were finally retained. This data-driven approach allowed us to identify common functional networks in the full cohort, exploiting temporal concatenation to maximize detectability of temporal variance in each network (46) while compensating for relatively short scan acquisition length (47).

2.4. Characterizing individual dFC networks

Dual regression was used to reconstruct individual functional networks in two steps (48). First, the chosen components were regressed into each processed functional dataset to determine a set of 7 time-courses per subject. Second, individual time-courses were regressed into their processed functional dataset to finally characterize 7 network spatial maps per subject. These 7 spatial maps are hereinafter defined static FC networks. For each subject, the 7 time-courses were used to calculate dFC networks. The first step in dual regression returned 616 (88 subjects \otimes 7 networks) time-courses, which were detrended and orthogonalized to head-motion displacements (29). Afterwards, these were used to calculate voxel-wise temporal coupling maps (i.e. voxel-to-network correlations) between each subject's preprocessed BOLD-EPI image and each network time-courses by means of Pearson's correlations (29).

A sliding-window approach (**Figure 1A**) was implemented to calculate dFC (i.e., to visualize spatial reconfigurations in temporal coupling maps over time). Each window covered 110s of spontaneous BOLD oscillations (50TR) such that its length exceeded the processed signal largest wavelength (49), meanwhile the sliding step size was determined as the highest temporal resolution available (1TR=2.2s) to study progressive evolution of dFC and produce a statistically large number of temporal coupling maps (N=132) for each subject and network (50) (**Figure 1B, atop**). Spatial dFC variation maps were then calculated voxelwise using the L1 norm distance (sum of absolute

differences) between each two consecutive temporal coupling maps, which were then summed up to obtain a unique image for subject and network. In other words, this measure accounts for spatial variations in voxel-to-network coupling over time (sliding-window correlations) for each voxel, network and subject (**Figure 1C, atop**).

In Matlab R2019a, a texture analytic method was furthermore implemented to measure the spatiotemporal changeover in dFC for each subject and network (29) (**Figure 1B, at bottom**). First, Pearson's correlations were discretized into 10 equal bins. For clarity, this discretization considered the full Pearson's correlation range (from -1 to 1), hence both positive and negative temporal coupling, with each bin covering a 0.2 step in such range. Spatiotemporal dFC transition matrices (10x10) were so defined as the cumulative frequency of cross-bin voxel transits between each consecutive sliding window per subject and network (**Figure 1C, at bottom**). Spatiotemporal dFC transitions were finally normalized by their maximum value. Spatial dFC variation maps and spatiotemporal dFC transition matrices provide complementary perspectives of brain dynamism: while the former localizes variations in functional networks voxelwise, the latter describes how these occur over time (29).

2.5. Statistical analyses

Statistical analysis was performed in Matlab R2019a. A chi-squared test was conducted to evaluate the proportion of gender distribution across the two samples. Age (in years) and head-motion (mean FD) were tested using two sample t-tests. Two-sample t-tests were conducted between groups to evaluate MDD effects in spatial dFC variation, for each network separately. In MDD patients, brain-behavior relationships were evaluated running analyses of covariance (ANCOVA) between spatial dFC variation and total, as well as sub-dimensional (i.e., sadness, negative thoughts, detachment and neurovegetative symptoms) MADRS scores, for each network separately. Age, gender, mean FD and study dataset were considered scalar confounding regressors in all analytic models.

The same analyses were conducted to identify spatiotemporal dFC transition patterns associated with MDD, and assess covarying relationships between dFC transitions and total or sub-dimensional MADRS scores in patients only, for each network separately. In this case, ANCOVAs were run for each matrix cell, factoring out main linear effects associated with MDD diagnosis, depression severity or MDD symptom subfactor, respectively. Age, gender, mean FD and study dataset were also factored out as scalar confounds. The same analyses were reiterated also controlling for pharmacological treatment effects in AO-MDD patients. In this analysis, continuous and categorical factors determined the hierarchy model for the sum of squares. Bivariate correlations across all variables followed by the Levine's and Shapiro-Wilk tests were conducted for each ANCOVA to assure that all assumptions were always met. Statistical significance level was set to $p < .05$ and multiple comparisons were counteracted using the Holm–Bonferroni method (FWER, $\alpha = .05$, $p < .001$).

3. Results

3.1. Depression severity

Both patient and control groups showed comparable demographical characteristics (**Table 1**). Mean FD showed modest head movements (< 0.25 mm) which did not differ between groups. In average, total MADRS scores indicated overall mild-to-moderate depression severity across MDD patients (**Table 1**). There was no statistical difference in mean depression severity between first-episode 16 ± 10 (M \pm SD) and recurrent MDD patients 17 ± 12 (M \pm SD), $t(33) = -0.54$, $p = .6$. There was a statistically significant difference in mean depression severity between pharmacologically treated 13 ± 10 (M \pm SD) and untreated MDD patients 21 ± 11 (M \pm SD), $t(32) = 2.4$, $p = .02$.

3.2. Spatial dynamic variations in AO-MDD

The automatic selection of static gICA maps successfully identified all 7 canonical networks which contribute to the intrinsic functional connectome (45) (**Figure 2**). Spatial dFC variations were overall reduced in AO-MDD (**Figure 3**) when compared to healthy controls in prefrontal cortical regions across several networks ($p < .005$, uncorrected). Spatial dFC variations were decreased in the lateral prefrontal cortex (IPFC) and middle frontal gyri (MFG) in all dFC networks whereas the DMN, Limbic and salience networks also involved ventromedial PFC (vmPFC) regions, such as the orbitofrontal cortex (OFC). Visual and somatomotor network dynamics were not affected by the disorder and thus excluded from further examinations. A detailed list of results can be found in **Table 2**.

Spatial dFC variations in the Limbic and DMN also showed reversed relationships with total and sub-dimensional MADRS scores in patients ($p < .05$, FDR corrected), with negative thoughts linked to DMN dynamics (**Table 3**). In contrast, sadness showed positive relationships with Limbic and DMN dynamics in the subgenual nucleus and Precuneal regions, respectively. The clinical relevance of these networks would have been overlooked by static FC, which instead highlights a

prominent involvement of the FPN (**Supplemental Table 1**).

3.3. Spatiotemporal dFC transitions and associations with symptomatology

Spatiotemporal dFC transitions were defined for all the remaining rs-fMRI networks but statistically significant differences in mean dFC transitions as a function of MDD diagnosis ($F(1,81) > 11.6$) were only found in recurrent coupling reconfigurations of the limbic network (**Figure 4**). These reconfigurations involved negative coupling areas which modulate the transitions across multiple dynamic states. In this network, spatiotemporal dFC transitions underlying negative network coupling were significantly scaling along total MADRS scores in patients ($F(1,27) > 13.6$). When considering MADRS dimensions, only the limbic network exhibited significant associations between spatiotemporal dFC transitions and the dimension of sadness ($F(1,27) > 13.6$). These transitions implied an intense shift towards positive dynamic coupling, indicating network excessive recruitment (**Figure 4**).

In the DMN, there were significant associations between spatiotemporal dFC transitions and negative thoughts ($F(1,27) > 13.6$). These involved both recurrent reconfigurations and minimally changing patterns during network negative coupling. Recurrent spatial reconfigurations in the FPN significantly scaled with neurovegetative symptoms ($F(1,27) > 13.6$). There was no significant relationship between spatiotemporal dFC transitions and the detachment dimension in any network: the DAN and salience network were not associated to AO-MDD.

4. Discussion

This spatially dynamic rs-fMRI study explored time-varying patterns in functionally parcellated, spatially distributed human brain networks to assess their temporal evolution in AO-MDD severity and symptom heterogeneity. The functional chronnectome allowed to quantify voxelwise temporal variations and spatiotemporal transitions across consecutive sliding windows for seven personalized networks obtained within an ICA framework. This methodology revealed that 1) multiple networks functionally interconnected in the PFC are affected in AO-MDD; 2) the limbic network is the foremost affected circuitry whose dynamics specifically link to depression severity; 3) across-subject symptom variability is associated with changes within specific functional networks.

4.1. Prefrontal functional dynamicity in adolescence-onset MDD.

If earlier functional chronnectome applications had shown increased brain dynamicity in psychiatric disorders like schizophrenia (29), here they showed prefrontal inflexibility (i.e., reduced dynamicity) in young MDD patients. This is consistent with recent functional dFC studies of unmedicated MDD and bipolar disorder adult patients (51), confirming the pivotal role of frontal lobe function in these disorders and favoring the development of transdiagnostic models in psychiatry (52). To our knowledge, no prior dFC study has investigated AO-MDD: on a speculative note, prefrontal inflexibility might subtend altered PFC maturation during adolescence that would persist in early adulthood (53).

Most functional networks showed dynamic inflexibility within the IPFC, whereas the OFC was inflexible in the DMN and salience networks, and the anterior cingulate cortex (ACC) only in the limbic network. The IPFC and OFC play a critical role in top-down cognitive control, a process that requires multiple networks involvement (54) whereas the ACC integrates affective and cognitive processes to facilitate response selection (55). We speculate that dFC inflexibility reveals network communication failure due to the tirelessly recruitment of IPFC in an unsuccessful attempt to

regulate persistent negative emotions (56), subsequently leading to loss of interest in previously pleasant events or lack of volition (57).

Fundamentally, dynamic inflexibility here expresses prefrontal lobe dysfunction, analogously to measurements of brain glucose metabolism and blood flow (58). The functional connectome could therefore enhance non-invasively and non-expensively existing imaging biomarkers to characterize and typify the neurobiology of AO-MDD and its course onward (53, 59).

4.2. Adolescence-onset MDD and limbic network dynamics.

The limbic network and the DMN are hierarchically integrated during the resting state (60, 61). The OFC component of the limbic network is implicated in processing instinctive emotions, motivation and affiliative behaviors related to social cohesion (62) which would afterwards be coordinated and integrated into cognition by the DMN through the ACC (63, 64). Present findings are in accordance with theoretical models of MDD where bottom-up affective content is not passed on to cognitive top-down examination and control (64, 65). Since its onset, MDD biochemical distortions upset this intrinsic functional organization, inducing some networks to hijack control over others. Spatiotemporal dFC transitions in patients implicate larger limbic isolation in the functional connectome due to subcortical pathophysiology (66, 67). Consistently with this model, our dFC quantifications showed altered limbic reconfigurations, which are necessary to merge with other networks and convey processed visceral emotion to cortical regions through the ACC.

4.3. Spatiotemporal dynamics as neuroimaging correlate of depression severity.

This study also evaluated dFC measures as probable imaging endpoints of MDD. Among various depression rating scales, we chose the MADRS to measure MDD severity (37). Our choice was motivated by the tool's wide usage in clinical practice as a clinician-rated instrument to assess depression severity on symptoms that promptly respond to treatment and antidepressant medication (38). dFC relationships were furthermore investigated along four-factor MADRS symptom

subclasses to differentially target cognitive and affective symptoms (38). Spatial dFC variations demonstrated a reversed relationship with total MADRS scores (i.e. depression severity) in both the Limbic and DMN networks in the inferior temporal gyrus and inferior parietal lobule. These regions have been implicated in some studies of depressed patients (68).

4.3.1. Dynamic limbic coupling reflects MDD severity.

There was a tight relation between spatiotemporal dFC transitions and total MADRS scores in the limbic network only. This finding confirms the pivotal role of subcortical circuitries in AO-MDD and links limbic inflexibility to depression severity (69, 70). These relationships concerned minimal temporal variations in negative coupling content. Therefore, MDD would only partially affect the dynamic spatial reconfigurations of the limbic network, in particular affecting those circuits which are negatively correlated to the limbic component while leaving the rest unaffected. Alternatively, it may be that negative and positive coupled regions in the functional chronnectome present differential temporal characteristics and that, at the current temporal resolution, dynamic transitions in positive coupling remain insensitive to catch inflexible limbic dynamicity. In perspective, such abnormal limbic integration may help distinguish functionally impairing clinical depressions from milder not-disabling cases, and prepare support accordingly (71).

4.3.2. Network - symptom associations in AO-MDD.

When investigating different MDD symptom clusters, spatiotemporal dFC transitions showed network-symptom specific associations, indicating that the limbic network, the DMN, the salience and the FPN have separable roles in MDD-related symptoms. Maladaptive communications among these networks in MDD have already been linked with negative emotions reflected in mood, as well as speech, facial expression and posture (18).

Here, spatiotemporal dFC transitions within the limbic network were associated with abnormal sadness. These involved regions characterized by large variations in their content that tend to

progressively minimize negative coupling over time. This finding is consistent with emotion regulation models that involve lower limbic structures to direct expressive and affective emotional components in MDD (72, 73). Present findings suggest that negative emotions in AO-MDD do not emerge as direct consequence of obstructed cortico-limbic integration but from incomplete limbic reconfigurations and consequent “crystallization” of functional dynamics as part of limbic segregation and isolation.

In addition, spatiotemporal coupling transitions within the DMN were related to pessimistic and suicidal thoughts, intended as thoughts of guilt, inferiority, remorse and ruin (the MADRS items do not consider actual suicidal attempts). These symptoms, characterized by persistence of internally directed attention, have consistently been linked to DMN activity (74, 75) and dynamics (34). In the DMN too, these spatiotemporal transitions dominated negative coupled circuits, reflecting delayed integration in the functional connectome and thus its inability to efficiently control high self-critical thoughts, when functional interactions are unbalanced or ill-coordinated with bottom-up processing (64). Moreover, unsteady FPN dynamics, characterized by delayed spatiotemporal reconfigurations, were related to somatic symptoms of MADRS that could reflect inhibitory control and anticipatory anxiety, which would disrupt higher cognitive functions and goal-oriented behavior.

The triple-network framework (55) assumes that cross-network interactions among the DMN, FPN and salience networks are characteristic of the healthy functional connectome. A recent dFC study demonstrated decreased dFC between the DMN and FPN in 51 unmedicated MDD (51). Our findings similarly suggest that lack of brain dynamicity between these two networks is actually relevant in the early stages of MDD both in adolescents and young adults (53).

Although spatial dFC variations were significantly inflexible in the salience network, no relationships between spatiotemporal dFC transitions and symptoms were observed. Evidence suggests that the salience network is implicated in anxiety disorders and anxiety comorbid with MDD (76, 77). However, the MADRS structure does not consider mental tension and panic as an

independent symptom class, which in some measures explains our findings. Furthermore, this network likely plays a greater role in addiction behavior or delusional (55) psychotic experiences (78) which are present only in severe forms of MDD.

4.4. Technical aspects and limitations

Although mean FD was factored out when examining brain-behavior relationships, head-motion could still specifically confound non-stationary dFC transitions (79). We therefore examined whether FD spikes were accounted for by image preprocessing (**Supplemental Figure1**) and conducted a parallel analysis using an artifactual motion component (**Supplemental Figure2**). Choosing an optimal sliding-window length is vital to identify neural dynamic patterns in rs-fMRI data (80). This holds true even in harmonized multisite protocols that use same acquisition/receiver head-coils to prevent MRI background noise from invalidating neural dFC detectability.

In this neuroimaging study, we took a novel spatial functional chronnectome model to investigate brain function dynamicity in AO-MDD patients and explore relationships with depression severity and symptoms. Nevertheless, there are other chronnectome models such as dynamic hierarchical approaches which could further elucidate between-network temporal relationships (81). Due to sample medication variability, some clinically relevant information might have been cancelled out: this might concern the salience network (benzodiazepine) or the DMN (SSRI). However, when including treatment as covariate we found the same functional pattern. Between-group differences in vigilance states might potentially lessen the specificity of our results (82). Independent measures of wakefulness are recommended in future clinical dFC studies of psychiatric disorders. The MADRS is a clinician-rated tool which monitors depression severity and treatment efficacy. However, it was not systematically administered in healthy controls, whom are typically administered as self-rated questionnaires. This might lessen dFC specificity to AO-MDD and needs independent confirmatory investigations. In particular, longitudinal studies could clarify whether brain dynamicity in MDD is linked to structural maturation (83) and follow treatment effects on

different symptom clusters.

4.5. Conclusion

In sum, this is the first functional chronnectome study to provide evidence for a dynamic imbalance between limbic, FPN and DMN in adolescence-onset MDD patients using rs-fMRI. This dynamic imbalance could underlie symptom variability not detected by the static FC approach. Distinct limbic network dynamics were related to sadness and severity of depression, while DMN dynamics were linked to negative thoughts.

Acknowledgements

Nicolas Dantchev, MD, is acknowledged for contributing access to patient included in Hôtel-Dieu Hospital, Paris. The Strasbourg University (SATT Conectus) is acknowledged for sponsorship of the study in adults with MDD, and Sainte-Anne Hospital, Paris, for sponsorship of the adolescent depression study. This work was supported by the ANR [ANR-12-SAMA-0004]; the Assistance-Publique-Hôpitaux-de-Paris and INSERM (interface grant); Paris-Descartes-University (collaborative-project-2010); Paris-Sud-University [IDEX-2012]; the European Union-funded FP6 Integrated Project IMAGEN [LSHM-CT-2007-037286]; the Eranet Neuron [ANR-18-NEUR00002-01-ADORe]; the Fondation de l'Avenir [AP-RM-17-013], the Fondation de France [00081242]; the Fédération pour la Recherche sur le Cerveau; the Fondation pour la Recherche Médicale [DPA20140629802].

Disclosures

The authors report no biomedical financial interests or potential conflicts of interest.

References

1. Kessler RC, Berglund P, Demler O, Jin R, Koretz D, Merikangas KR et al. The epidemiology of major depressive disorder: results from the National Comorbidity Survey Replication (NCS-R). *JAMA* 2003; 289(23): 3095-3105.
2. Kennedy SH. Core symptoms of major depressive disorder: relevance to diagnosis and treatment. *Dialogues Clin Neurosci* 2008; 10(3): 271-277.
3. Andrade L, Caraveo-Anduaga JJ, Berglund P, Bijl RV, De Graaf R, Vollebergh W et al. The epidemiology of major depressive episodes: results from the International Consortium of Psychiatric Epidemiology (ICPE) Surveys. *Int J Methods Psychiatr Res* 2003; 12(1): 3-21.
4. Zisook S, Lesser I, Stewart JW, Wisniewski SR, Balasubramani GK, Fava M et al. Effect of age at onset on the course of major depressive disorder. *Am J Psychiatry* 2007; 164(10): 1539-1546.
5. Merikangas KR, Nakamura EF, Kessler RC. Epidemiology of mental disorders in children and adolescents. *Dialogues Clin Neurosci* 2009; 11(1): 7-20.
6. Gusnard DA, Akbudak E, Shulman GL, Raichle ME. Medial prefrontal cortex and self-referential mental activity: relation to a default mode of brain function. *Proc Natl Acad Sci U S A* 2001; 98(7): 4259-4264.
7. Greicius MD, Flores BH, Menon V, Glover GH, Solvason HB, Kenna H et al. Resting-state functional connectivity in major depression: abnormally increased contributions from subgenual cingulate cortex and thalamus. *Biol Psychiatry* 2007; 62(5): 429-437.
8. Fitzgerald PB, Laird AR, Maller J, Daskalakis ZJ. A meta-analytic study of changes in brain activation in depression. *Hum Brain Mapp* 2008; 29(6): 683-695.
9. Kaiser RH, Andrews-Hanna JR, Wager TD, Pizzagalli DA. Large-Scale Network Dysfunction in Major Depressive Disorder: A Meta-analysis of Resting-State Functional Connectivity. *JAMA Psychiatry* 2015; 72(6): 603-611.

10. Zhang K, Zhu Y, Zhu Y, Wu S, Liu H, Zhang W et al. Molecular, Functional, and Structural Imaging of Major Depressive Disorder. *Neurosci Bull* 2016; 32(3): 273-285.
11. Takamura T, Hanakawa T. Clinical utility of resting-state functional connectivity magnetic resonance imaging for mood and cognitive disorders. *J Neural Transm (Vienna)* 2017; 124(7): 821-839.
12. Connolly CG, Wu J, Ho TC, Hoeft F, Wolkowitz O, Eisendrath S et al. Resting-state functional connectivity of subgenual anterior cingulate cortex in depressed adolescents. *Biol Psychiatry* 2013; 74(12): 898-907.
13. Smitha KA, Akhil Raja K, Arun KM, Rajesh PG, Thomas B, Kapilamoorthy TR et al. Resting state fMRI: A review on methods in resting state connectivity analysis and resting state networks. *Neuroradiol J* 2017; 30(4): 305-317.
14. Kupfer DJ, Frank E, Phillips ML. Major depressive disorder: new clinical, neurobiological, and treatment perspectives. *Lancet* 2012; 379(9820): 1045-1055.
15. Shou H, Yang Z, Satterthwaite TD, Cook PA, Bruce SE, Shinohara RT et al. Cognitive behavioral therapy increases amygdala connectivity with the cognitive control network in both MDD and PTSD. *Neuroimage Clin* 2017; 14: 464-470.
16. Mulders PC, van Eijndhoven PF, Schene AH, Beckmann CF, Tendolkar I. Resting-state functional connectivity in major depressive disorder: A review. *Neurosci Biobehav Rev* 2015; 56: 330-344.
17. Brakowski J, Spinelli S, Dorig N, Bosch OG, Manoliu A, Holtforth MG et al. Resting state brain network function in major depression - Depression symptomatology, antidepressant treatment effects, future research. *J Psychiatr Res* 2017; 92: 147-159.
18. Sheline YI, Price JL, Yan Z, Mintun MA. Resting-state functional MRI in depression unmasks increased connectivity between networks via the dorsal nexus. *Proc Natl Acad Sci U S A* 2010; 107(24): 11020-11025.

19. Manoliu A, Meng C, Brandl F, Doll A, Tahmasian M, Scherr M et al. Insular dysfunction within the salience network is associated with severity of symptoms and aberrant inter-network connectivity in major depressive disorder. *Front Hum Neurosci* 2013; 7: 930.
20. Zhang S, Chen JM, Kuang L, Cao J, Zhang H, Ai M et al. Association between abnormal default mode network activity and suicidality in depressed adolescents. *BMC Psychiatry* 2016; 16(1): 337.
21. Shen Y, Yao J, Jiang X, Zhang L, Xu L, Feng R et al. Sub-hubs of baseline functional brain networks are related to early improvement following two-week pharmacological therapy for major depressive disorder. *Hum Brain Mapp* 2015; 36(8): 2915-2927.
22. Huang X, Huang P, Li D, Zhang Y, Wang T, Mu J et al. Early brain changes associated with psychotherapy in major depressive disorder revealed by resting-state fMRI: evidence for the top-down regulation theory. *Int J Psychophysiol* 2014; 94(3): 437-444.
23. Crowther A, Smoski MJ, Minkel J, Moore T, Gibbs D, Petty C et al. Resting-state connectivity predictors of response to psychotherapy in major depressive disorder. *Neuropsychopharmacology* 2015; 40(7): 1659-1673.
24. Insel T, Cuthbert B, Garvey M, Heinssen R, Pine DS, Quinn K et al. Research domain criteria (RDoC): toward a new classification framework for research on mental disorders. *Am J Psychiatry* 2010; 167(7): 748-751.
25. Peng D, Yao Z. Neuroimaging Advance in Depressive Disorder. *Adv Exp Med Biol* 2019; 1180: 59-83.
26. Calhoun VD, Miller R, Pearlson G, Adali T. The chronnectome: time-varying connectivity networks as the next frontier in fMRI data discovery. *Neuron* 2014; 84(2): 262-274.
27. Abrol A, Chaze C, Damaraju E, Calhoun VD. The chronnectome: Evaluating replicability of dynamic connectivity patterns in 7500 resting fMRI datasets. *Conf Proc IEEE Eng Med Biol Soc* 2016; 2016: 5571-5574.

28. Zabelina DL, Andrews-Hanna JR. Dynamic network interactions supporting internally-oriented cognition. *Curr Opin Neurobiol* 2016; 40: 86-93.
29. Iraj A, Deramus TP, Lewis N, Yaesoubi M, Stephen JM, Erhardt E et al. The spatial chronnectome reveals a dynamic interplay between functional segregation and integration. *Hum Brain Mapp* 2019; 40(10): 3058-3077.
30. Sheehan DV, Lecrubier Y, Sheehan KH, Amorim P, Janavs J, Weiller E, Hergueta T, Baker R, Dunbar GC. The Mini-International Neuropsychiatric Interview (M.I.N.I.): the development and validation of a structured diagnostic psychiatric interview for DSM-IV and ICD-10. *J Clin Psychiatry*. 1998;59
31. Bassett DS, Wymbs NF, Porter MA, Mucha PJ, Carlson JM, Grafton ST. Dynamic reconfiguration of human brain networks during learning. *Proc Natl Acad Sci U S A* 2011; 108(18): 7641-7646.
32. Shine JM, Koyejo O, Poldrack RA. Temporal metastates are associated with differential patterns of time-resolved connectivity, network topology, and attention. *Proc Natl Acad Sci U S A* 2016; 113(35): 9888-9891.
33. Liu J, Liao X, Xia M, He Y. Chronnectome fingerprinting: Identifying individuals and predicting higher cognitive functions using dynamic brain connectivity patterns. *Hum Brain Mapp* 2018; 39(2): 902-915.
34. Kaiser RH, Whitfield-Gabrieli S, Dillon DG, Goer F, Beltzer M, Minkel J et al. Dynamic Resting-State Functional Connectivity in Major Depression. *Neuropsychopharmacology* 2016; 41(7): 1822-1830.
35. Wu X, He H, Shi L, Xia Y, Zuang K, Feng Q et al. Personality traits are related with dynamic functional connectivity in major depression disorder: A resting-state analysis. *J Affect Disord* 2019; 245: 1032-1042.

36. Long Y, Cao H, Yan C, Chen X, Li L, Castellanos FX et al. Altered resting-state dynamic functional brain networks in major depressive disorder: Findings from the REST-meta-MDD consortium. *Neuroimage Clin* 2020; 102163.
37. Montgomery SA, Asberg M. A new depression scale designed to be sensitive to change. *Br J Psychiatry* 1979; 134: 382-389.
38. Quilty LC, Robinson JJ, Rolland JP, Fruyt FD, Rouillon F, Bagby RM. The structure of the Montgomery-Asberg depression rating scale over the course of treatment for depression. *Int J Methods Psychiatr Res* 2013; 22(3): 175-184.
39. Radloff LS: The CES-D scale: A self report depression scale for research in the general population. *App Psychol Measur* 1977,1:385-401.
40. Revah-Levy, A., Birmaher, B., Gasquet, I. *et al.* The Adolescent Depression Rating Scale (ADRS): a validation study. *BMC Psychiatry* 7, 2 (2007).
41. Cox RW. AFNI: software for analysis and visualization of functional magnetic resonance neuroimages. *Comput Biomed Res* 1996; 29(3): 162-173.
42. Jenkinson M, Beckmann CF, Behrens TE, Woolrich MW, Smith SM. Fsl. *Neuroimage* 2012; 62(2): 782-790.
43. Marchitelli R, Minati L, Marizzoni M, Bosch B, Bartres-Faz D, Muller BW et al. Test-retest reliability of the default mode network in a multi-centric fMRI study of healthy elderly: Effects of data-driven physiological noise correction techniques. *Hum Brain Mapp* 2016; 37(6): 2114-2132.
44. Power JD, Barnes KA, Snyder AZ, Schlaggar BL, Petersen SE. Spurious but systematic correlations in functional connectivity MRI networks arise from subject motion. *Neuroimage* 2012; 59(3): 2142-2154.
45. Yeo BT, Krienen FM, Sepulcre J, Sabuncu MR, Lashkari D, Hollinshead M et al. The organization of the human cerebral cortex estimated by intrinsic functional connectivity. *J Neurophysiol* 2011; 106(3): 1125-1165.

46. Allen, E. A., Damaraju, E., Plis, S. M., Erhardt, E. B., Eichele, T., & Calhoun, V. D. (2014). Tracking whole-brain connectivity dynamics in the resting state. *Cerebral cortex (New York, N.Y.: 1991)*, 24(3), 663–676.
47. Hindriks R et al. Can sliding-window correlations reveal dynamic functional connectivity in resting-state fMRI? *Neuroimage* 2015; 127: 242-256.
48. Nickerson LD, Smith SM, Ongur D, Beckmann CF. Using Dual Regression to Investigate Network Shape and Amplitude in Functional Connectivity Analyses. *Front Neurosci* 2017; 11: 115.
49. Leonardi N, Van De Ville D. On spurious and real fluctuations of dynamic functional connectivity. *Neuroimage* 2015; 104: 430-436.
50. Allen EA, Damaraju E, Plis SM, Erhardt EB, Eichele T, Calhoun VD. Tracking whole-brain connectivity dynamics in the resting state. *Cereb Cortex* 2014; 24(3): 663-676.
51. Wang J, Wang Y, Huang H, Jia Y, Zheng S, Zhong S et al. Abnormal dynamic functional network connectivity in unmedicated bipolar and major depressive disorders based on the triple-network model. *Psychol Med* 2020; 50(3): 465-474.
52. Chen X, Liu C, He H, Chang X, Jiang Y, Li Y et al. Transdiagnostic differences in the resting-state functional connectivity of the prefrontal cortex in depression and schizophrenia. *J Affect Disord* 2017; 217: 118-124.
53. Kerestes R, Davey CG, Stephanou K, Whittle S, Harrison BJ. Functional brain imaging studies of youth depression: a systematic review. *Neuroimage Clin* 2014; 4: 209-231.
54. Miller EK. The prefrontal cortex and cognitive control. *Nat Rev Neurosci* 2000; 1(1): 59-65.
55. Menon V. Large-scale brain networks and psychopathology: a unifying triple network model. *Trends Cogn Sci* 2011; 15(10): 483-506.
56. Mayberg HS. Modulating dysfunctional limbic-cortical circuits in depression: towards development of brain-based algorithms for diagnosis and optimised treatment. *Br Med Bull* 2003; 65: 193-207.

57. Nitschke JB, Mackiewicz KL. Prefrontal and anterior cingulate contributions to volition in depression. *Int Rev Neurobiol* 2005; 67: 73-94.
58. Videbech P. PET measurements of brain glucose metabolism and blood flow in major depressive disorder: a critical review. *Acta Psychiatr Scand* 2000; 101(1): 11-20.
59. Yan B, Xu X, Liu M, Zheng K, Liu J, Li J et al. Quantitative Identification of Major Depression Based on Resting-State Dynamic Functional Connectivity: A Machine Learning Approach. *Front Neurosci* 2020; 14: 191.
60. Buckner RL, Andrews-Hanna JR, Schacter DL. The brain's default network: anatomy, function, and relevance to disease. *Ann N Y Acad Sci* 2008; 1124: 1-38.
61. Catani M, Dell'acqua F, Thiebaut de Schotten M. A revised limbic system model for memory, emotion and behaviour. *Neurosci Biobehav Rev* 2013; 37(8): 1724-1737.
62. Mesulam MM. From sensation to cognition. *Brain* 1998; 121 (Pt 6): 1013-1052.
63. Carhart-Harris RL, Friston KJ. The default-mode, ego-functions and free-energy: a neurobiological account of Freudian ideas. *Brain* 2010; 133(Pt 4): 1265-1283.
64. Northoff G, Wiebking C, Feinberg T, Panksepp J. The 'resting-state hypothesis' of major depressive disorder-a translational subcortical-cortical framework for a system disorder. *Neurosci Biobehav Rev* 2011; 35(9): 1929-1945.
65. Feinberg TE. *From Axons to Identity: Neurological Explorations of the Nature of the Self*. 1st ed WW Norton & Company 2009.
66. Ito H, Kawashima R, Awata S, Ono S, Sato K, Goto R et al. Hypoperfusion in the limbic system and prefrontal cortex in depression: SPECT with anatomic standardization technique. *J Nucl Med* 1996; 37(3): 410-414.
67. Mega MS, Cummings JL, Salloway S, Malloy P. The limbic system: an anatomic, phylogenetic, and clinical perspective. *J Neuropsychiatry Clin Neurosci* 1997; 9(3): 315-330.

68. Wise, T., Radua, J., Via, E. *et al.* Common and distinct patterns of grey-matter volume alteration in major depression and bipolar disorder: evidence from voxel-based meta-analysis. *Mol Psychiatry* 22, 1455–1463 (2017).
69. Seminowicz DA, Mayberg HS, McIntosh AR, Goldapple K, Kennedy S, Segal Z *et al.* Limbic-frontal circuitry in major depression: a path modeling metanalysis. *Neuroimage* 2004; 22(1): 409-418.
70. Hamon M, Blier P. Monoamine neurocircuitry in depression and strategies for new treatments. *Prog Neuropsychopharmacol Biol Psychiatry* 2013; 45: 54-63.
71. Paris J. The mistreatment of major depressive disorder. *Can J Psychiatry* 2014; 59(3): 148-151.
72. Park C, Rosenblat JD, Lee Y, Pan Z, Cao B, Iacobucci M *et al.* The neural systems of emotion regulation and abnormalities in major depressive disorder. *Behav Brain Res* 2019; 367: 181-188.
73. Ramasubbu R, Konduru N, Cortese F, Bray S, Gaxiola-Valdez I, Goodyear B. Reduced intrinsic connectivity of amygdala in adults with major depressive disorder. *Front Psychiatry* 2014; 5: 17.
74. Sheline YI, Barch DM, Price JL, Rundle MM, Vaishnavi SN, Snyder AZ *et al.* The default mode network and self-referential processes in depression. *Proc Natl Acad Sci U S A* 2009; 106(6): 1942-1947.
75. Jacob Y, Morris LS, Huang KH, Schneider M, Rutter S, Verma G *et al.* Neural correlates of rumination in major depressive disorder: A brain network analysis. *Neuroimage Clin* 2020; 25: 102142.
76. Stein MB, Simmons AN, Feinstein JS, Paulus MP. Increased amygdala and insula activation during emotion processing in anxiety-prone subjects. *Am J Psychiatry* 2007; 164(2): 318-327.

77. Coplan JD, Aaronson CJ, Panthangi V, Kim Y. Treating comorbid anxiety and depression: Psychosocial and pharmacological approaches. *World J Psychiatry* 2015; 5(4): 366-378.
78. Pelletier-Baldelli A, Andrews-Hanna JR, Mittal VA. Resting state connectivity dynamics in individuals at risk for psychosis. *J Abnorm Psychol* 2018; 127(3): 314-325.
79. Laumann TO et al. On the stability of BOLD fMRI correlations. *Cerebral Cortex* 2017; 27: 4719-4732.
80. Zalesky A, Breakspear M. Towards a statistical test for functional connectivity dynamics. *Neuroimage*. 2015 Jul 1; 114:466-70.
81. Iraj A, Fu Z, Damaraju E, DeRamus TP, Lewis N, Bustillo JR et al. Spatial dynamics within and between brain functional domains: A hierarchical approach to study time-varying brain function. *Hum Brain Mapp* 2019; 40(6): 1969-1986.
82. Haimovici, A., Tagliazucchi, E., Balenzuela, P. *et al.* On wakefulness fluctuations as a source of BOLD functional connectivity dynamics. *Sci Rep* 7, 5908 (2017).
83. Rubia K. Functional brain imaging across development. *Eur Child Adolesc Psychiatry* 2013; 22(12): 719-731.

Figure legends

Figure 1: Calculation of dynamic functional connectivity. (A) The figure summarizes the dFC coupling analysis for a given subject and its network (e.g. the limbic network). Functional network coupling using Pearson's correlations was calculated voxelwise between preprocessed resting-state BOLD data (the pink voxel signal) and limbic ICA time-course (the red signal) within 132 sliding windows. (B) This analysis returned 132 dynamic coupling maps voxelwise for that subject and its network. Voxels' transitions across consecutive coupling maps (e.g. the pink voxel) were calculated across ten equal-width discretized subsets (pink numbers) and stored in a transition matrix. (C) At top, the total sum of the absolute differences across each two consecutive coupling maps returned the dFC variability map whereas at bottom, the overall sum across all voxels determined the spatiotemporal dFC transitions for that subject and network. The matrix counter diagonal hosts minimally variable dynamics concerning positive (2nd quadrant) or negative (3rd quadrant) connectivity, comparable to static functional networks. As transitions leave this diagonal their variability increases, being the largest at opposite corners. Dynamic transitions in the 1st and 4th quadrants imply a change in correlation sign, which underlies spatiotemporal reconfigurations occurring through network dynamic states. dFC: dynamic functional connectivity; BOLD: blood-oxygen level-dependent; ICA: independent component analysis.

Figure 2. Group functional networks probed in the study. The figure shows the spatiotemporal characteristics of seven rs-fMRI functional networks selected out of 20 independent components. For each network, the spatial distribution of (anti-)correlations ($z \geq \pm 2.3$; $p < .001$) is overlaid on the MNI template. Next on the right, the power spectrum (0.01 - 0.1 Hz) validates the neural nature of the selected component. In the same plot, the percent similarity index (ρ) to external template and total grey matter (GM) is also reported. For each of these networks, their time-course was reconstructed in each subject using dual regression methods. This was then used as input for dFC analysis. rs-fMRI: resting-state functional magnetic resonance imaging; gICA: group independent

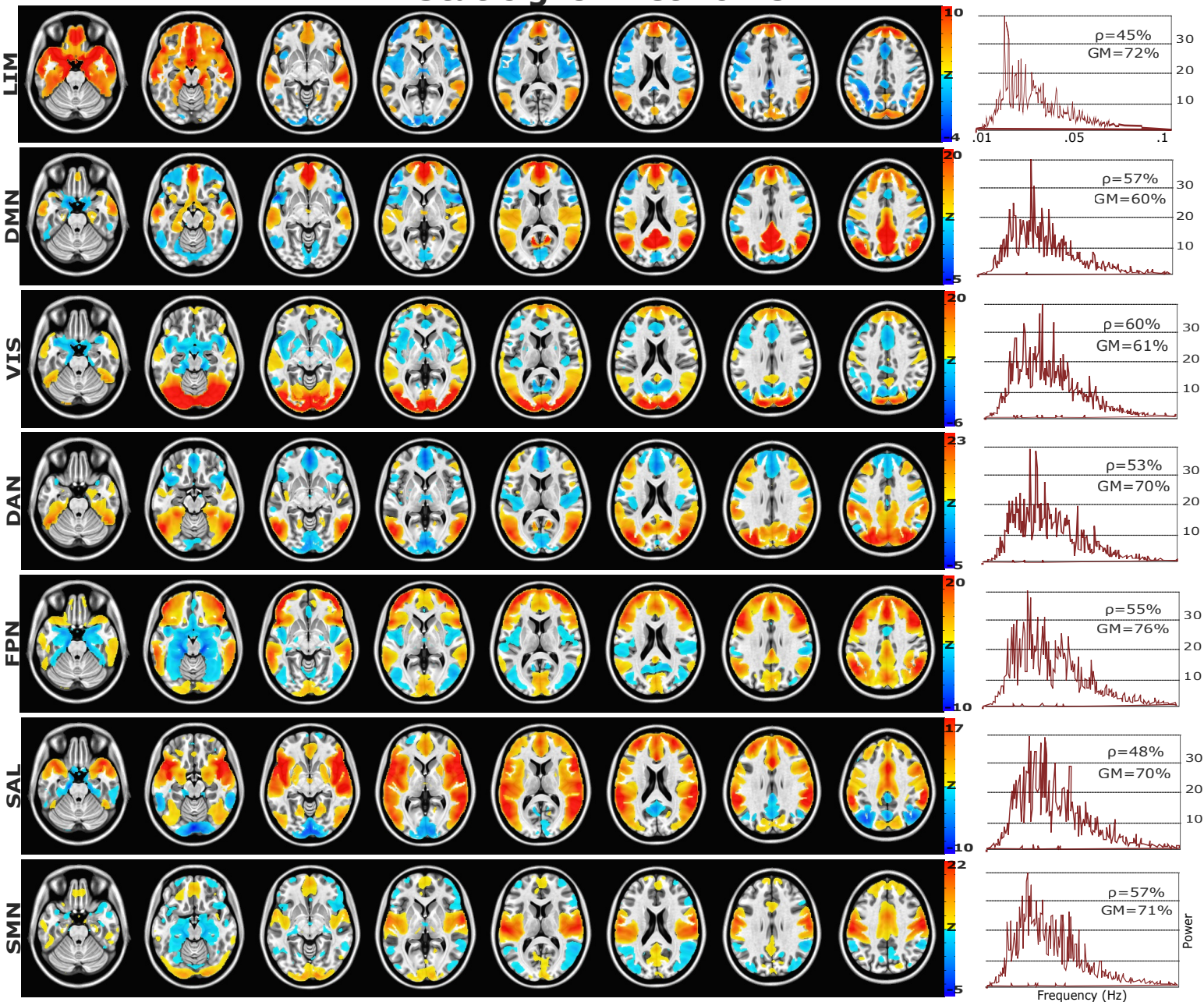
component analysis; GM: grey matter; dFC: dynamic functional connectivity; LIM: limbic network; DMN: default-mode network; VIS: visual network; DAN: dorsal-attention network; FPN: frontoparietal network; SAL: salience network; SMN: somatomotor network.

Figure 3. dFC variability maps within networks and MDD diagnosis effects. For each rs-fMRI network, dorsal and medial surface-projected dFC variability maps averaged across healthy subjects (left), MDD patients (middle) and two-sample student t-tests between groups (right) are presented. Left: spatiotemporal inflexibility is denoted by blue colors while high dynamicity is denoted by hot colors, as readily visible in the visual and somatomotor networks; FOV limitations bias reduces dFC variability on top brain images. Middle: MDD patients' inflexibility is apparent in the functional chronnectome. Right: statistical results indicate that all but visual and somatomotor networks are affected by MDD, in the PFC, precuneus, temporal and occipital regions (uncorrected, $p < 0.005$, $t > \pm 2.9$). MDD: major depressive disorder; dFC: dynamic functional connectivity; PFC: prefrontal cortex; DMN: default-mode network; FPN: frontoparietal network; DAN: dorsal-attention network.

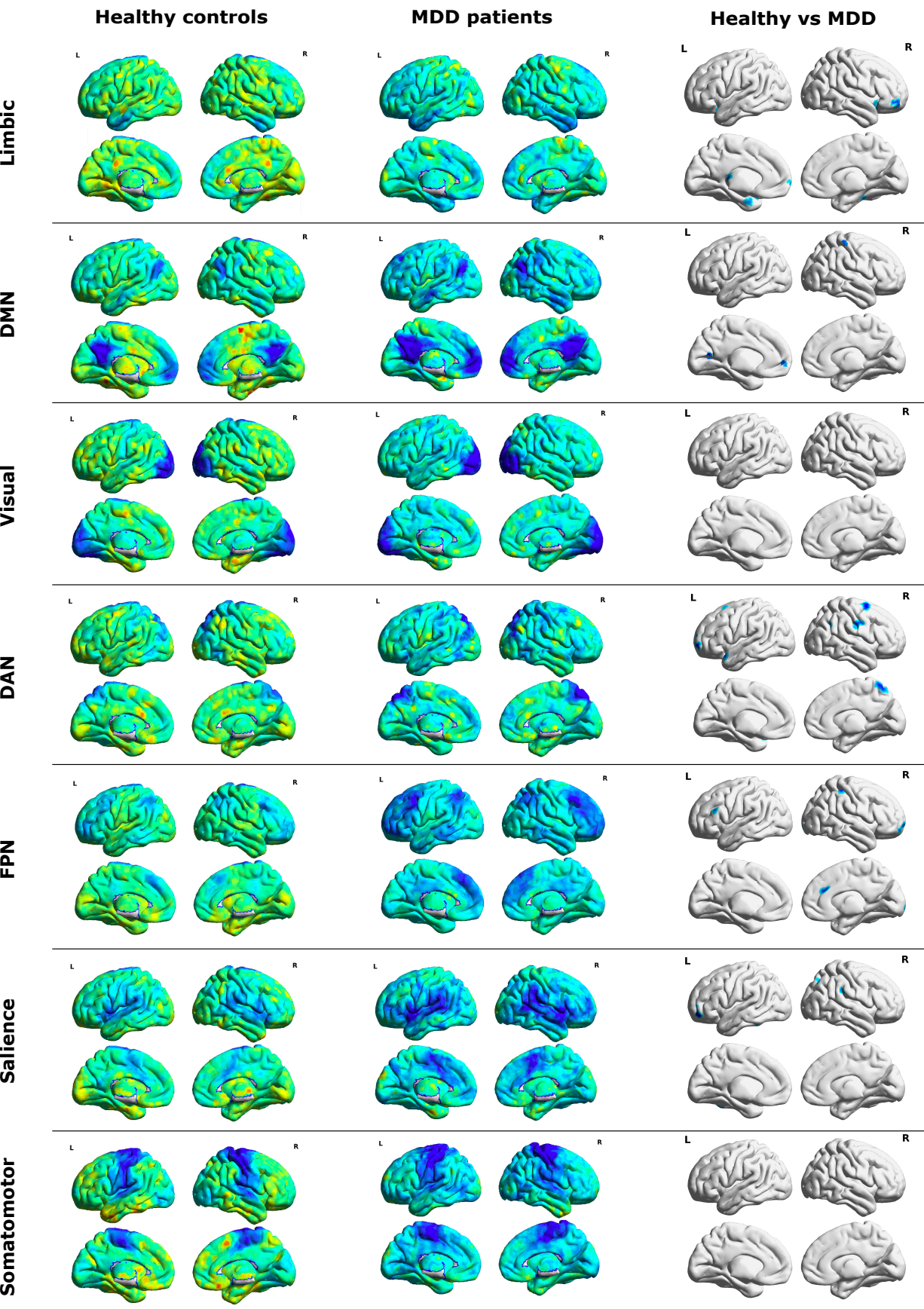
Figure 4. Main spatiotemporal dFC transition results. (Top) The figure shows mean spatiotemporal dFC transitions across all participants for five rs-fMRI networks. The distribution of cross-bin voxel transits is the largest (in yellow) on the counter diagonal to progressively lessen towards opposite corners (in blue), consistently across all rs-fMRI networks. The maximum is typically located upper-right, where positive correlations reside and networks reach their steady state (i.e. segregation). The bottom-left area represents network decoupling dynamics (i.e. negative correlations) associated with inter-network integration. Each triangular matrix (see Figure1, bottom left) represents non-stationary processes where spatial reconfigurations occur as network transits across these brain states. The upper-left and bottom right corners reflect excessive change in network dynamics unlikely to reflect neural dynamism but rather artifacts. (Bottom) The figure

shows statistically corrected results from neurobehavioral analysis: MDD alters spatiotemporal reconfigurations in the limbic network dynamics (MDD diagnosis) with disease severity related to limbic decoupling (MADRS). Abnormal sadness is related to hyper-recruitment of the limbic system (Sadness); excessive negative thoughts are related to DMN alterations (Negative thoughts), whereas spatiotemporal FPN reconfigurations are related to vegetative subdimension. rs-fMRI: resting-state functional MRI; dFC: dynamic functional connectivity; MDD: major depressive disorder; DMN: default-mode network; DAN: dorsal-attention network; FPN: frontoparietal network.

Static gICA networks



Spatial dFC variation

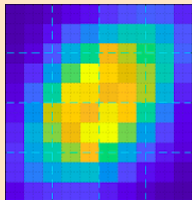


2 Mean Variation 99

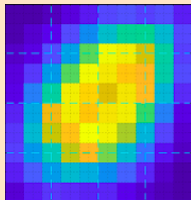
-2 MDD < HC -7

Spatiotemporal dFC transitions

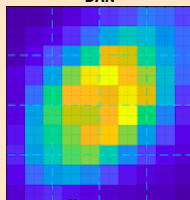
Limbic network



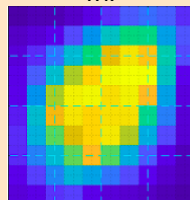
DMN



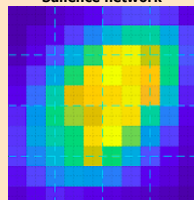
DAN



FPN



Saliency network



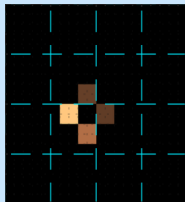
% transitions



Neurobehavioral analysis

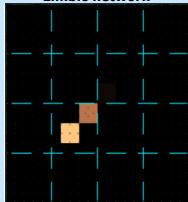
MDD diagnosis

Limbic network



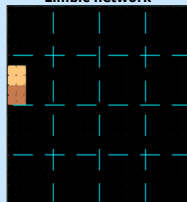
MADRS

Limbic network



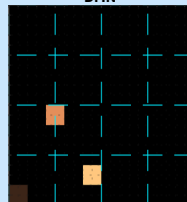
Sadness

Limbic network



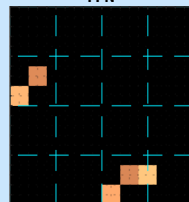
Negative Thoughts

DMN



Neurovegetative

FPN



	<i>AO-MDD patients (N=35)</i>	<i>Healthy controls (N=53)</i>	<i>Across-sample statistics</i>
<i>Age</i>	<i>21 ± 6 (15 – 36)</i>	<i>20 ± 3 (16 – 28)</i>	<i>t(86) = -.7, p = .46</i>
<i>Gender</i>	<i>21 (60%)</i>	<i>33 (62%)</i>	<i>χ²(1, N=88) = .05, p = .8</i>
<i>MADRS</i>	<i>17 ± 11 (2 - 41)</i>	<i>2 ± 3 (0 – 9) (N=24/53)</i>	-
<i>ADRS</i>	-	<i>.4 ± .7 (0 – 2) (N=27/53)</i>	-
<i>CES-D</i>	-	<i>8.2 ± 8 (0 – 35) (N=24/53)</i>	-
<i>Head-motion</i>	<i>.1 ± .08 (.03 – .25)</i>	<i>.08 ± .07 (.02 – .25)</i>	<i>t(86) = -.9, p = .35</i>
<i>Disease onset</i>	<i>16 ± 3 (11 – 21)</i>		

Table 1. Epidemiological and Functional Imaging Characteristics. The table reports descriptive statistics for demographic, psychometric and functional imaging characteristics (first column) in both samples (second and third columns). Values are summarized by mean and standard deviation within each group. The range of their values is also provided in parenthesis. Across-sample statistical evaluations are reported in the last column. Age and disease onset are reported in years. Gender reports the percentage of female individuals. Head-motion indicates in-scanner mean FD in millimeters. AO-MDD: adolescent-onset major depressive disorder; MADRS: Montgomery–Åsberg Depression Rating Scale scores; ADRS: Adolescent Depression Rating Scale; CES-D: Centre for Epidemiological Studies Depression; FD: framewise displacement.

<i>Functional Network</i>	<i>Cluster size</i>	<i>Centroid</i>			<i>Cluster value</i>	<i>Brain Region</i>
		<i>x</i>	<i>y</i>	<i>z</i>		
<i>Limbic</i>	96	-42.5	-52.1	-7.4	-3.6551	<i>BA11</i>
	54	-40.3	-18.5	-11.7	-4.1251	<i>BA13</i>
	32	8	-64.3	-1.3	-4.0282	<i>BA10</i>
	31	18.3	-0.5	-29.6	-3.757	<i>Amygdala</i>
<i>DMN</i>	43	4.1	65.3	11.5	-3.9101	<i>BA23</i>
	34	37.8	-33	-15.3	-3.952	<i>BA11</i>
	29	6.9	-57.3	-1.4	-3.5376	<i>BA10</i>
<i>DAN</i>	184	-31.5	-4.2	62.5	-4.6306	<i>BA6</i>
	154	-50.3	11.2	13.4	-4.2957	<i>BA13</i>
	109	-60.6	9.2	34.2	-3.8761	<i>BA6</i>
	86	25.8	-64.7	-3.1	-3.9551	<i>BA10</i>
	39	-58.2	58.4	31.6	-4.5012	<i>BA40</i>
	29	24.4	-52.4	12.8	-4.377	<i>BA10</i>
<i>FPN</i>	61	-7.7	-32.1	26.3	-3.6419	<i>BA32</i>
	44	-20.8	-69.8	-3.6	-3.7134	<i>BA10</i>
	32	-24.4	-58.8	-8.3	-3.5482	<i>BA10</i>
<i>Salience</i>	123	38.1	-54.9	-9.9	-4.5252	<i>BA11</i>
	82	-37.6	68	43.2	-3.7285	<i>BA11</i>
	39	-24.3	-49.7	20.6	-4.0637	<i>BA10</i>
	39	-59.3	35.2	28.8	-3.8003	<i>BA40</i>

Table 2. Main regions characterized by spatial dFC inflexibility in AO-MDD. For each functional network, the table reports the spatial cluster size (in number of voxels), centroid (in RAI coordinates) and mean value (t-score) for regions characterized by reduced spatial dFC variations in AO-MDD ($p < .005$). Brodmann areas are also herein reported for clarity. All networks showed dynamic inflexibility in the lateral PFC (BA10) whereas Limbic, DMN and salience networks showed reduced dFC variations in the ventromedial PFC (BA11). Only the limbic network showed reduced dFC variations in the Amygdala, whereas the anterior (BA32) and middle (BA23) cingulate showed inflexible dynamics in the FPN and DMN, respectively. Superior frontal (BA6) reductions were observed only in the DAN, which shared reductions with the Salience network in the Inferior parietal lobule (BA40). Reduced dFC variability was also found in the insula (BA13) for the limbic network and the DAN. No statistically significant effects were observed for the visual and somatomotor network. dFC: dynamic functional connectivity; (AO)-MDD: (adolescence-onset) major depressive disorder; RAI: right-anterior-posterior; PFC: prefrontal cortex; OFC: orbitofrontal cortex; DMN: default-mode network; FPN: frontoparietal network; DAN: dorsal-attention network.

Functional Network	MADRS component	Cluster size	Centroid			Cluster value	Brain Region
			x	y	z		
Limbic	Total	564	-38	77	17	-4.4581	BA39
	Detachment	433	-40	75	15	-4.2143	BA39
	Sadness	494	0.8	-47	-14	4.1271	BA25
	Vegetative	1150	37	43	53	-4.8508	BA40
DMN	Total	976	37	68	42	-3.4205	BA39/7
		649	56	58	-5	-4.6925	BA37
	Detachment	465	55	8	6	-4.0018	BA22
		464	56	56	-7	-4.6742	BA37
	Negative thoughts	1436	-2	59	30	-3.6308	BA7
		1120	36	67	41	-3.9274	BA39
		1000	54	62	-5	-5.198	BA37
	Sadness	1039	39	63	41	4.1891	BA7
Vegetative	970	-50	40	50	-4.2026	BA40	

Table 3. Spatial relationships between network dFC variations and MADRS scores. Spatial cluster size (in number of voxels), centroid (in RAI coordinates) and mean score (t-values) for sensitive regions to depression severity and symptom factors in the functional chronnectome. Only the DMN and Limbic networks show sensitivity to MADRS scores and symptoms ($p < .05$, FDR corrected). Both dFC networks scale with depression severity in middle temporal parietal regions (BA39/37/7). The same regions are associated with detachment symptoms in both networks, and negative thoughts only in the DMN. Sadness scaled with anterior and posterior cingulate regions in the Limbic and DMN, respectively. Neurovegetative symptoms were linked to dynamics in the inferior parietal lobule/supramarginal gyrus (BA40). Negative t-values indicate a reversed directionality between spatial dFC variations and MADRS scores. dFC: dynamic functional connectivity; MADRS: Montgomery-Asberg Depression Rating Scale; RAI: right-anterior-posterior; DMN: default-mode network; BA: Brodmann's area.